Non–Small Cell Lung Cancer Staging: Efficacy Comparison of Integrated PET/CT versus 3.0-T Whole-Body MR Imaging[1]

Chin A Yi, MD
Kyung Min Shin, MD
Kyung Soo Lee, MD
Byung-Tae Kim, MD
Hojoong Kim, MD
O Jung Kwon, MD
Joon Young Choi, MD
Myung Jin Chung, MD

Purpose: To compare prospectively the diagnostic efficacies of integrated positron emission tomography (PET)/computed tomography (CT) and 3.0-T whole-body magnetic resonance (MR) imaging for determining TNM stages in non–small cell lung cancer (NSCLC).

Materials and Methods: Institutional review board approval and informed consent were obtained. The study included 165 patients (125 men, 40 women; mean age, 61 years) with NSCLC proved at pathologic examination who underwent both unenhanced PET/CT and whole-body MR imaging. Pathologic findings for T (n = 123) and N (n = 150) staging and pathologic or follow-up imaging findings (n = 154) for M staging were reference standards. The efficacies of PET/CT and whole-body MR imaging for lung cancer staging were compared by using the McNemar test.

Results: Primary tumors (n = 123 patients) were correctly staged in 101 (82%) patients at PET/CT and in 106 (86%) patients at whole-body MR imaging (P = .263). N stages (n = 150 patients) were correctly determined in 105 (70%) patients at PET/CT and in 102 (68%) patients at whole-body MR imaging (P = .880). Thirty-one (20%) of 154 patients had metastatic lesions. Accuracy for detecting metastases was 86% (133 of 154 patients) at PET/CT, and that at whole-body MR imaging was 86% (132 of 154 patients) (P > .99). Although the differences were not statistically significant, whole-body MR imaging was more useful for detecting brain and hepatic metastases, whereas PET/CT was more useful for detecting lymph node and soft-tissue metastases.

Conclusion: Both PET/CT and 3.0-T whole-body MR imaging appear to provide acceptable accuracy and comparable efficacy for NSCLC staging, but for M-stage determination, each modality has its own advantages.

[1] From the Department of Radiology and Center for Imaging Science (C.A.Y., K.M.S., K.S.L., M.J.C.), Department of Nuclear Medicine (B.T.K., J.Y.C.), and Division of Pulmonary and Critical Care Medicine, Department of Medicine (H.K., O.J.K.), Samsung Medical Center, Sungkyunkwan University School of Medicine, 50, Ilwon-Dong, Kangnam-Ku, Seoul 135-710, Korea. From the 2007 RSNA Annual Meeting. Received October 18, 2007; revision requested January 10, 2008; revision received February 25; accepted March 7; final version accepted March 19. Supported by Samsung Medical Center Clinical Research Development Program grant #CRDP CRS 106-41-2. **Address correspondence to** K.S.L. (e-mail: *kyungs.lee@samsung.com*).

Optimal lung cancer treatment relies on accurate disease staging, which is based on tumor size and extent, regional nodal involvement, and the presence of metastasis. Although thoracic computed tomography (CT) has been considered the standard modality of choice for the assessment of intrathoracic spread of lung cancer (1), no consensus has been reached concerning metastasis evaluation. Fluorine 18 fluorodeoxyglucose (FDG) positron emission tomography (PET) was introduced and developed as an integrated modality for accurate nodal staging and for metastatic lesion detection in the whole body (2–7). Currently, integrated PET/CT, by providing both morphologic and metabolic features, appears to have better efficacy for staging lung cancer than CT alone or PET alone (8,9).

Whole-body magnetic resonance (MR) imaging has become feasible and enables fast imaging throughout the body (10–12). This technique is based on real-time gradient-echo imaging and a sliding table platform (rolling table concept, which eliminates time-consuming repositioning of patients and surface coils). The latest generation of MR imagers has a high field strength of more than 1.5 T and is reported to have upgraded capabilities in terms of temporal and spatial resolution due to improved signal-to-noise ratios with high magnetic field strength conditions (13,14).

Because both integrated PET/CT and whole-body MR imaging can provide whole-body imaging, both modalities are used for staging a malignant condition in patients. According to a study (15), the diagnostic efficacy of PET/CT is superior to that of whole-body MR imaging for T and N staging and similar to that of whole-body MR imaging for the detection of metastases. However, according to another study (16), whole-body MR imaging had better sensitivity than PET/CT for the detection of metastatic lesions. In these studies (15,16), in which a 1.5-T MR unit was used, the regional nodal or metastatic lesions were from various types of primary malignancies with a wide range of tumor stages. The purpose of our study was to compare prospectively the diagnostic efficacies of integrated PET/CT and 3.0-T whole-body MR imaging for determining TNM stages in patients with non–small cell lung cancer (NSCLC).

Advances in Knowledge

- Both PET/CT and 3.0-T whole-body MR imaging appear to provide acceptable accuracy and comparable efficacy for non–small cell lung cancer (NSCLC) staging, but for M-stage determination, each modality has its own advantages.
- Whole-body MR imaging is more useful for detecting brain and hepatic metastases, whereas PET/CT is more useful for detecting lymph node and soft-tissue metastases.

Materials and Methods

Our institutional review board approved our study, and informed consent was obtained from all patients for this prospective study.

Patients

From July 2005 to August 2006, a total of 174 consecutive patients with NSCLC proved at pathologic examination underwent both PET/CT (Discovery LS; GE Medical Systems, Milwaukee, Wis) and whole-body MR imaging (Achieva; Philips Medical Systems, Best, the Netherlands) at a single tertiary referral hospital. Because bronchioloalveolar cell carcinoma usually did not have nodal or extrathoracic metastasis, we did not include patients with that tumor. None of these patients were suspected of having metastatic disease at clinical examination (physical examination, laboratory findings at admission, and enhanced thoracic CT scans covering the thorax and upper abdomen). Data collection was performed prospectively in consecutive patients. PET/CT and MR imaging were performed within a 4-day interval (mean interval, 1.6 days; range, 0–4 days). Nine patients were excluded for the following reasons: seven had contraindications to MR imaging due to pacemakers or other metallic implants, and two could not complete MR imaging because of claustrophobia. Therefore, 165 patients (125 men, 40 women; mean age, 61 years ± 10 [standard deviation]; age range, 34–82 years), 113 of whom had been evaluated in a study involving the diagnostic efficacy of 3.0-T thoracic MR imaging for hilar and mediastinal nodal staging (17), were included in the study (Fig 1). The male-to-female ratio and mean age of our patients were representative of those of patients in the Korean Central Cancer Registry (male-to-female ratio, 76:24; mean age, 62.4 years ± 9.3 in 2002).

Implication for Patient Care

- Both PET/CT and 3.0-T whole-body MR imaging appear to provide acceptable accuracy and comparable efficacy for NSCLC staging, but for M-stage determination, each modality has its own advantages; therefore, whole-body MR/PET may be the future imaging modality for NSCLC staging, especially for M staging, although state-of-the-art multisection CT remains the study of choice for T staging.

Published online before print
10.1148/radiol.2482071822

Radiology 2008; 248:632–642

Abbreviations:
CI = confidence interval
FDG = fluorine 18 fluorodeoxyglucose
NSCLC = non–small cell lung cancer
TSE = turbo spin echo

Author contributions:
Guarantor of integrity of entire study, K.S.L.; study concepts/study design or data acquisition or data analysis/interpretation, all authors; manuscript drafting or manuscript revision for important intellectual content, all authors; manuscript final version approval, all authors; literature research, all authors; clinical studies, all authors; statistical analysis, C.A.Y., K.M.S., K.S.L.; and manuscript editing, all authors

Authors stated no financial relationship to disclose.

See also the article by Ohno et al in this issue.

Image Acquisition

PET/CT imaging.—Detailed imaging methods were described in previous reports (9,18). Briefly, the glucose level in the peripheral blood was 150 mg/dL [8.33 mmol/L] or lower in all patients. Patients received an intravenous injection of 370 MBq (10 mCi) of FDG and then rested for more than 45 minutes before undergoing scanning. Scans were acquired by using a PET/CT device (Discovery LS; GE Healthcare, Milwaukee, Wis), which consisted of a PET scanner (Advance NXi; GE Healthcare) and an eight-section CT scanner (LightSpeed Plus; GE Healthcare). Immediately after unenhanced CT was performed, emission PET was performed in the identical transverse field of view. Coregistered images were displayed by using software (Xeleris; GE Healthcare). It took approximately 35 minutes to complete a PET/CT study.

Whole-body MR imaging.—All MR studies were performed with a 3.0-T imager (Achieva; Philips Medical Systems). A sensitivity-encoding cardiac coil (Philips Medical Systems) with a six-coil element was used to obtain dedicated transverse images of the thorax, whereas a body coil with a four-coil element (built in the bore) was used to obtain whole-body images.

The dedicated transverse imaging technique of the thorax was described in a previous report (14). Briefly, for T2-weighted images, a breath-hold T2-weighted triple-inversion black-blood turbo spin-echo (TSE) sequence was employed with cardiac gating. For T1-weighted images, a T1-weighted three-dimensional multishot turbo field-echo sequence was used during breath holding.

For whole-body coronal reformatted images, eight or nine stacks of contiguous coronal images were obtained by using both fat-suppressed T2-weighted TSE and enhanced T1-weighted three-dimensional turbo field-echo sequences. To obtain enhanced turbo field-echo images, a paramagnetic contrast agent (Magnevist; Schering, Berlin, Germany) was administered intravenously with a bolus injection technique at a dose of 0.2 mmol per kilogram of body weight. In addition to coronal images, we also obtained additional sagittal (covering the cervical, thoracic, and upper lumbar spine) and transverse (covering the lower lumbar spine and pelvic bones) T1-weighted TSE images to readily depict bone metastatic lesions (Table 1). It took approximately 40 minutes to complete a whole-body MR imaging study.

Image Evaluation

PET/CT imaging.—Integrated PET/CT images were evaluated jointly by a chest radiologist (K.S.L., with 18 years of CT interpretation experience) and a nuclear medicine physician (B.T.K., with 4 years of PET/CT interpretation experience) with consideration of diagnostic criteria for a positive finding as shown in Table 2 (19). Both were unaware of whole-body MR imaging findings and of clinical and pathologic evaluation results.

Tumor staging was performed with consideration of the size, involvement of surrounding organ or chest wall, and distance from the carina of the primary tumor. The nodal station was evaluated and allocated to 10 groups, according to the lymph node map definition for lung cancer staging proposed by Mountain and Dresler (20). All lymph nodes in the thorax and extrathoracic regions with abnormal FDG uptake (greater than mediastinal blood pool uptake) in the extrathoracic regions were considered to be metastatic, unless they showed high attenuation (>70 HU) or benign calcification (central nodular, laminated, popcornlike, or diffuse) on unenhanced CT images. An abnormal focal FDG uptake that accompanied a corresponding anatomic alteration was considered to be indicative of metastasis (9,18). Subcentimeter lung nodules, regardless of FDG uptake (usually less than mediastinal blood pool uptake), were considered malignant when they were greater than 10 in number (21–23). Any nodule more than 10 mm in diameter with FDG uptake more than that of the mediastinal blood pool was considered malignant (Table 2) (24).

Whole-body MR imaging.—Two chest radiologists (C.A.Y. and K.M.S., each with 2 years of experience in whole-body MR image analysis) interpreted sequential MR images immediately after the examination. It took approximately 30 minutes to analyze whole-body MR

Figure 1

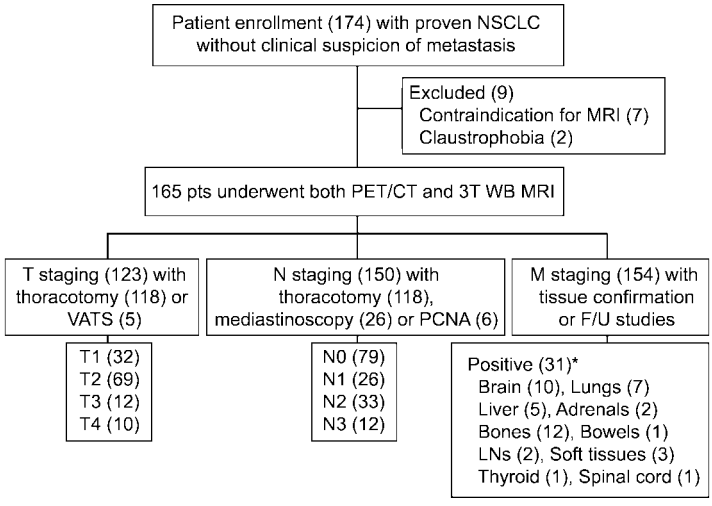

Figure 1: Flowchart shows how patients were enrolled, how TNM staging was determined, and what the stages were. *F/U* = follow-up, *LNs* = lymph node metastases, *PCNA* = percutaneous needle aspiration biopsy of supraclavicular nodes, *pts* = patients, *VATS* = video-assisted thoracoscopic surgery, *WB* = whole body. * = Because one patient had more than one organ metastasis, numbers for each organ add up to more than 31.

images. When the two chest radiologists were confronted with difficulty in the evaluation of extrathoracic organs, they asked musculoskeletal or neuroimaging radiologists for help with interpretation. Decisions on findings were reached by consensus. Both were unaware of PET/CT imaging findings and of clinical and pathologic evaluation results. Tumor and nodal staging were performed as for PET/CT, by using dedicated transverse images of the thorax. Nodes with high signal intensity and eccentric cortical thickening or obliterated fatty hilum on T2-weighted triple-inversion black-blood TSE images were considered malignant (17). During MR imaging evaluations, the presence of a metastatic lesion was determined from an assessment of tumor morphologic characteristics and its pattern of contrast enhancement. Discrete lesions with high signal intensity on T2-weighted TSE images were considered to be metastatic, particularly when the lesions demonstrated substantial enhancement on three-dimensional turbo field-echo images. Extrathoracic lymph nodes were regarded to contain malignancy when they showed high signal intensity with eccentric cortical thickening or obliterated fatty hilum on T2-weighted TSE images, regardless of their size. Central necrosis on enhanced T1-weighted images was also considered a sign of a malignant node, irrespective of size (Table 2).

Reference Standard

Histopathologic cell types of primary tumors were confirmed in all patients ($n = 165$) with findings from percutaneous needle aspiration biopsy ($n = 16$) or surgery ($n = 149$). Pathologic T and N stages were available for 123 and 150 patients, respectively. T stages were determined by using thoracotomy results (lobectomy results in 93 patients, bilobectomy results in 10, and pneumonectomy results in 15) in 118 patients and video-assisted thoracoscopic surgery resec-

Table 1

MR Imaging Parameters

Imaging Area	Imaging Protocol	Parameter	Coils Used	Time (min)
Dedicated thoracic				
	T1-weighted turbo field echo	Turbo field-echo factor, 0; turbo field-echo shot, 24 in radial turbo direction; repetition time msec/echo time msec, 3.0/1.49; flip angle, 10°; number of signals acquired, two; FOV, 400 mm; matrix, 224; SPAIR FS; sensitivity-encoding factor, two	Sensitivity-encoding cardiac, six-coil element	1.0
	T2-weighted TIBB	1200–1800/60 (effective); two R-R intervals; echo train length, 21; FOV, 400 mm; matrix, 256; section thickness, 5 mm with 1-mm intersection gap; SPIR FS; sensitivity-encoding factor, two		5.5–6.0
Whole body				
	T1-weighted turbo field echo	Turbo field-echo factor, 60; turbo field-echo shot, 185 in radial turbo direction; 3.0/1.44; flip angle, 10°; FOV, 470 mm (RFOV, 55%; stack overlap, 50 mm); matrix, 224; slab thickness, 220 mm, each slab divided into 44 partitions (5-mm section thickness); SPAIR FS	Body, four-coil element	6.0–7.0
	T2-weighted TSE	3631/80; echo train length, 22; FOV, 470 mm (RFOV, 55%; stack overlap, 50 mm); matrix, 256; section thickness, 8 mm with 1-mm intersection gap; SPAIR FS		8.5–9.5
Spine*	T1-weighted TSE	400/7.9; echo train length, four; FOV, 320 mm; matrix, 320; section thickness, 4 mm with 0.4-mm intersection gap	Body, four-coil element	5.0–5.5
Pelvis†	T1-weighted TSE	436/10; echo train length, four; FOV, 340 mm; matrix, 284; section thickness, 6 mm with 2-mm intersection gap		4.0–4.5

Note.—FOV = field of view, FS = fat saturation, RFOV = rectangular field of view, SPAIR = spectral presaturation attenuated inversion recovery, SPIR = spectral presaturation inversion recovery, TIBB = triple inversion black blood.

* Sagittal images covering the cervical, thoracic, and upper lumbar spine.

† Transverse images covering the lower lumbar spine and pelvic bones.

Table 2

Indications of Positive Findings at TNM Staging of NSCLC with Two Modalities

TNM Staging	Indicative Finding at PET/CT	Indicative Finding at 3.0-T Whole-Body MR Imaging
T stage		
T1	Tumors ≤ 3 cm or endobronchial nodule distal to segmental bronchus	Tumors ≤ 3 cm or endobronchial nodule distal to segmental bronchus
T2	Tumors > 3 cm or endobronchial nodule with obstructive pneumonia or atelectasis	Tumors > 3 cm or endobronchial nodule with obstructive pneumonia or atelectasis
T3	Tumors with mediastinal or chest wall invasion or tumors within main bronchus	Tumors with mediastinal or chest wall invasion or tumors within main bronchus
T4	Tumors with surrounding organ invasion or pleural seeding with or without effusion	Tumors with surrounding organ invasion or pleural seeding with or without effusion
N stage		
N1 (ipsilateral hilar)	FDG uptake more than that of mediastinal blood pool, without calcification or high attenuation	Eccentric cortical thickening or obliterated fatty hilum on T2-weighted TIBB images, irrespective of their sizes
N2 (ipsilateral mediastinal)	FDG uptake more than that of mediastinal blood pool, without calcification or high attenuation	Eccentric cortical thickening or obliterated fatty hilum on T2-weighted TIBB images, irrespective of their sizes
N3 (SCN or contralateral mediastinal)	FDG uptake more than that of mediastinal blood pool, without calcification or high attenuation	Eccentric cortical thickening or obliterated fatty hilum on T2-weighted TIBB images, irrespective of their sizes
M stage		
Brain	Focal FDG uptake more than that of surrounding parenchyma	Enhancing nodule on T1-weighted images*
Lungs	Subcentimeter nodules > 10 in number, irrespective of their FDG uptake, or any nodule with FDG uptake more than that of mediastinal blood pool	Subcentimeter nodules > 10 in number, irrespective of their signal intensities, or any enhancing nodule on T1-weighted images > 10 mm in diameter*
Liver	Focal FDG uptake more than that of surrounding parenchyma	Enhancing nodule on T1-weighted images*
Kidneys	Focal FDG uptake more than that of surrounding parenchyma	Enhancing nodule on T1-weighted images*
Adrenals	Focal FDG uptake more than liver uptake	Enhancing nodule on T1-weighted images, no fat suppression*
Bowels	Positive FDG uptake and bowel wall thickening†	Wall thickening or mass with enhancement
Bones	Focal FDG uptake more than liver uptake	Enhancing lesion on T1-weighted images*
Lymph nodes	Positive FDG uptake without calcification or high attenuation†	Eccentric cortical thickening or obliterated fatty hilum on T2-weighted or necrosis on T1-weighted images, irrespective of their sizes
Soft tissues	Focal FDG uptake more than liver uptake	Enhancing nodule on T1-weighted images*

Note.—SCN = supraclavicular nodes, TIBB = triple inversion black blood.

* Enhancing nodule on T1-weighted images, with high signal intensity on T2-weighted images.

† Positive uptake is focal uptake more than that of the liver.

tion results in five patients. N stages were determined in 150 patients, with thoracotomy results in 118 patients, with mediastinoscopy results in 26 patients, and with supraclavicular nodal biopsy results in six patients (Table 2).

Metastatic lesions, which could be evaluated in 154 patients, were found in 31 (20%) patients. Nine patients had lesions proved at pathologic examination. The remaining 22 patients (16 at the time of staging and six at follow-up studies) had metastatic lesions confirmed at specific organ-dedicated or follow-up imaging studies (ie, dedicated MR imaging at the time of staging in 16 patients, follow-up dedicated MR imaging in 10 patients, follow-up CT studies in five patients, follow-up PET/CT in five patients, and follow-up bone scan in 11 patients). In six patients in whom metastases were detected at follow-up imaging studies, the lesions were regarded as metastatic (grew from microscopic metastatic focus) because the primary cancers in these patients were resected at surgery after initial staging work-up.

In 13 patients, 16 sites were suspected to be metastatic at initial clinical-imaging studies at either PET/CT or

whole-body MR imaging. The absence of metastasis at these 16 sites was proved by using the following methods: biopsy (n = 1) of lesions in the liver suspected to be metastatic, surgical excision (n = 1) of an adrenal lesion, organ-specific multiphase CT (n = 4) in liver and adrenal lesions, bone scans (n = 4), dedicated conventional MR imaging (n = 4) of bone lesions, or ultrasonography (n = 2) of neck and muscular lesions. For the remaining 110 patients, findings of clinical follow-up studies served as reference standards for the determination of the absence of metastasis. The mean clinical follow-up time for these 110 patients was 592 days (range, 165–808 days). Follow-up studies performed after whole-body MR imaging and integrated PET/CT imaging studies consisted of clinical-laboratory evaluations, imaging follow-up studies, and histopathologic assessments.

Statistical Analysis

Statistical analyses were performed by using software (SPSS, version 10.1.4; SPSS, Chicago, Ill). Sensitivity, specificity, accuracy, and predictive values of PET/CT and whole-body MR imaging were calculated by using the standard definitions. Confidence intervals (CIs) were calculated for accuracy values on the basis of a 95% confidence level. The accuracies of PET/CT and whole-body MR imaging for TNM staging were determined, and differences between two modalities were evaluated by using the McNemar test. P values less than .05 were considered to indicate significant differences for all tests.

Post hoc power analysis by using the two-sided McNemar test was performed to determine whether the resultant sample size was of sufficient magnitude to support confidence in the outcome results. A minimum of 98 patients was required to detect a difference in terms of a power of .8 and a significance level of .05.

Figure 2

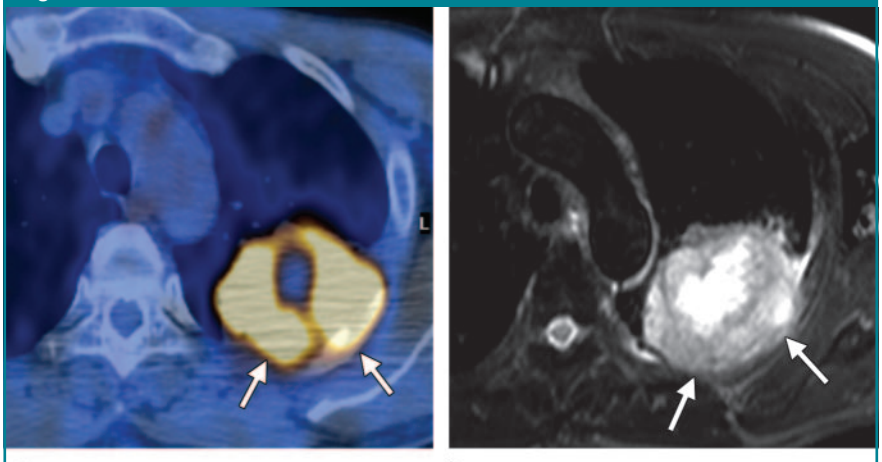

a. b.

Figure 2: Images of stage T3 squamous cell carcinoma of the lung in a 64-year-old man that was correctly staged at PET/CT and MR imaging. **(a)** Integrated PET/CT image shows 75-mm necrotic mass with high FDG uptake (maximum standardized uptake value = 14.6) in left upper lobe. Chest wall invasion of tumor (arrows) is overt. **(b)** Transverse T2-weighted triple-inversion black-blood MR image demonstrates high-signal-intensity lesion containing necrotic center. Note clearly visualized area of chest wall invasion (arrows). Thoracotomy results confirmed presence of chest wall invasion.

Results

The pathologic subtypes of lung cancers in the 165 included patients were as follows: adenocarcinoma in 86 patients, squamous cell carcinoma in 59 patients, unspecified NSCLC in nine patients, pleomorphic carcinoma in three patients, adenosquamous cell carcinoma in three patients, sarcomatoid carcinoma in three patients, and large cell neuroendocrine carcinoma in two patients.

Tumor Staging

The distribution of T stages determined with pathologic findings in 123 patients was as follows: T1 cancer in 32 patients, T2 in 69, T3 in 12, and T4 in 10. The primary tumor was correctly staged in 101 (82%) patients (95% CI: 75%,

Table 3

Detection and Staging of Primary Tumor at PET/CT and Whole-Body MR Imaging in 123 Patients with Lung Cancer

	PET/CT					3.0-T Whole-Body MR Imaging				
Pathologic Finding	T0*	T1	T2	T3	T4	T0*	T1	T2	T3	T4
T1 (n = 32)	1	29	2	0	0	1	30	1	0	0
T2 (n = 69)	0	6	62	1	0	0	4	58	4	3
T3 (n =12)	0	0	5	6	1	0	0	2	9	1
T4 (n = 10)	0	0	4	2	4	0	0	0	1	9
Total (n = 123)	1	35	73	9	5	1	34	61	14	13

Note.—Data are numbers of patients. The accuracy of integrated PET/CT was 82% (101 of 123 patients) and that of whole-body MR imaging was 86% (106 of 123 patients).

* One patient had T1 lung cancer that was not detected at either PET/CT or whole-body MR imaging.

89%) at PET/CT and in 106 (86%) patients (95% CI: 80%, 92%) at whole-body MR imaging (Fig 2). The difference in accuracies between integrated PET/CT and whole-body MR imaging was not statistically significant (P = .263, McNemar test) (Table 3).

Nodal Staging

A total of 712 nodal stations in 150 patients were evaluated with pathologic findings. Of these, 105 (15%) stations from 71 (47%) patients proved to be positive findings for malignancy. The distribution of N stages determined with pathologic findings was as follows: stage N0 in 79 patients, N1 in 26, N2 in 33, and N3 in 12. The N stage was correctly determined in 105 (70%) patients (95% CI: 63%, 77%) at PET/CT and in 102 (68%) (95% CI: 61%, 75%) at whole-body MR imaging (P = .880, McNemar test) (Table 4, Fig 3).

Efficacy of Whole-Body MR Imaging and PET/CT for Metastasis Detection

Metastatic lesions were confirmed in 43 organs in 31 (20%) of 154 patients. Of these 31 patients, 21 (68%) had one organ metastasis and 12 (39%) had a single lesion metastasis. Seven patients had N3 disease, 13 had N2 disease, three had N1 disease, and eight had N0 disease. (In these 31 patients, nodal stages were determined with pathologic findings in 20 patients and with clinical findings in 11 patients.) The diagnostic efficacies of the two modalities are summarized in Table 5. On a per-patient basis (n = 154), accuracy, sensitivity, and specificity were 86% (133 of 154 patients) (95% CI: 81%, 91%), 48% (15 of 31 patients), and 96% (118 of 123 patients), respectively, at PET/CT; at whole-body MR imaging, the corresponding values were 86% (132 of 154 patients) (95% CI: 81%, 91%), 52% (16 of 31 patients), and 94% (116 of 123 patients), respectively (P > .99, .625, > .99, respectively) (Table 5; Figs 4, 5).

Specific Organ Metastasis Detection

Bones were the most frequent site of metastasis (12 [8%] of 154 patients—single metastasis in five patients and multiple in seven patients). At both

Table 4

Detection and Staging of Nodal Metastasis at PET/CT and Whole-Body MR Imaging in 150 Patients with Lung Cancer

Pathologic Finding	PET/CT				3.0-T Whole-Body MR Imaging			
	N0	N1	N2	N3	N0	N1	N2	N3
N0 (n = 79)	72	4	2	1	65	6	8	0
N1 (n = 26)	15	8	3	0	10	10	5	1
N2 (n =33)	13	4	15	1	11	2	20	0
N3 (n = 12)	0	0	2	10	2	1	2	7
Total (n = 150)	100	16	22	12	88	19	35	8

Note.—Data are numbers of patients. The accuracy of integrated PET/CT was 70% (105 of 150 patients) and that of whole-body MR imaging was 68% (102 of 150 patients).

Figure 3

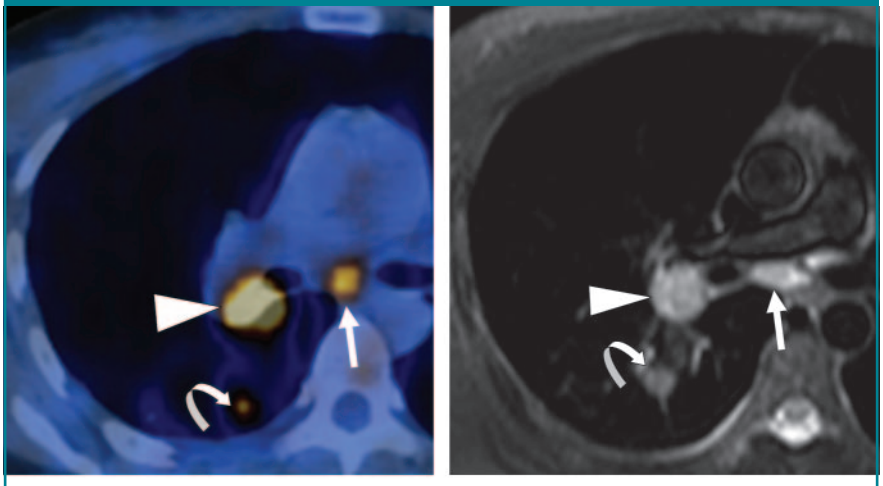

a. b.

Figure 3: Images of metastatic lymph nodes in nodal stations 7 (subcarinal nodes) and 10 (hilar nodes) in a 37-year-old woman with adenocarcinoma of the lung that were correctly staged at PET/CT and MR imaging. **(a)** Integrated PET/CT image shows high FDG uptake in subcarinal (arrow) (maximum standardized uptake value = 4.9) and right hilar (arrowhead) (maximum standardized uptake value = 10.1) nodes. Note portion of primary cancer (curved arrow) in right lower lobe. **(b)** Transverse T2-weighted triple-inversion black-blood MR image shows subcarinal (arrow) and right hilar (arrowhead) nodes with high signal intensity with obliteration of fatty hilum. Note primary cancer (curved arrow). Subcarinal and hilar nodes proved to contain cancer cells at mediastinoscopy and follow-up imaging study, respectively.

Table 5

Comparison of Diagnostic Efficacies of PET/CT and Whole-Body MR Imaging for M Staging

Parameter	PET/CT	3.0-T Whole-Body MR Imaging	P Value*
Sensitivity (%)	48 (15/31)	52 (16/31)	>.99
Specificity (%)	96 (118/123)	94 (116/123)	.625
Accuracy (%)	86 (133/154)	86 (132/154)	>.99
Positive predictive value (%)	75 (15/20)	70 (16/23)	. . .
Negative predictive value (%)	88 (118/134)	89 (116/131)	. . .

Note.—Data in parentheses are numbers used to calculate percentages. Data were calculated on a per-patient basis (n = 154 patients). Metastases were present in 31 patients.

* Determined by using the McNemar test.

PET/CT and whole-body MR imaging, metastatic foci were detected in eight (67%) patients. In four patients in whom bone metastases had not been detected, three had single metastasis. The metastases were confirmed later with bone biopsy findings in one patient, with follow-up PET/CT findings in two patients, and with follow-up CT findings in one patient, 3–9 months after surgical removal of the primary tumor. Whole-body MR imaging was more useful for detecting brain and hepatic metastases, whereas PET/CT was more useful for detecting lymph node and soft-tissue metastases. Brain metastases (15–30 mm in diameter) (in 10 [6%] patients) were detected at whole-body MR imaging in five (50%) patients, whereas they (30 mm in diameter) were detected in only one (10%) patient at PET/CT (Fig 5). In five patients in whom brain metastases had not been detected, one had a metastatic lesion (6 mm in diameter) detected at dedicated brain MR imaging at the time of lung cancer diagnosis and four had metastatic lesions confirmed at follow-up brain MR imaging, 4–10 months after lung cancer surgery. Whole-body MR imaging helped detect hepatic metastases (7–31 mm in diameter) in four (80%) of five patients, whereas unenhanced PET/CT did not help detect any of them. Three (60%) of five patients had hepatic metastatic lesions smaller than 10 mm in diameter. Prominent FDG uptake at lymph node and soft-tissue lesions allowed metastasis detection at PET/CT, although they were small in size (none of these were detected at whole-body MR imaging). Superficial location or small size of lymph node or soft-tissue metastases was a factor that contributed to not detecting the lesions at whole-body MR imaging.

Figure 4

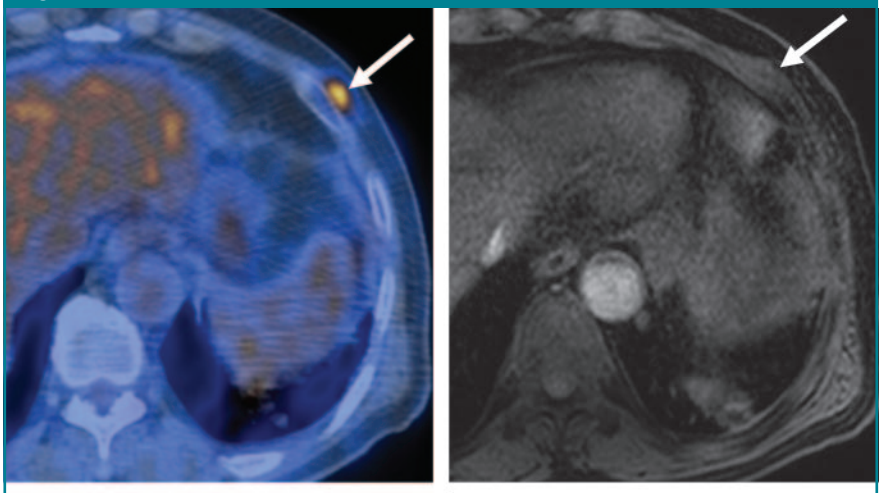

a. b.

Figure 4: Images of soft-tissue metastasis in left anterior chest wall in a 73-year-old man with squamous cell carcinoma of the lung (with negative finding for nodal metastasis, N0 disease) that was correctly detected at PET/CT but not at whole-body MR imaging. **(a)** Integrated PET/CT image demonstrates high FDG uptake within soft-tissue nodule (arrow) (maximum standardized uptake value = 5.4) in left anterior chest wall. **(b)** T1-weighted turbo field-echo MR image does not clearly demonstrate metastatic nodule. In retrospect, nodule (arrow) can be localized on this MR image. Excisional biopsy findings disclosed metastatic squamous cell carcinoma.

Table 6

True- and False-Positive Detection of Metastases in Organs Evaluated at PET/CT and Whole-Body MR Imaging

	True-Positive Cases		False-Positive Cases	
Location	PET/CT	3.0-T Whole-Body MR Imaging	PET/CT	3.0-T Whole-Body MR Imaging
Bone ($n = 12$)	8	8	5	4
Brain ($n = 10$)	1	5	0	0
Lungs ($n = 6$)	4	3	2	0
Liver ($n = 5$)	0	4	0	3
Soft tissues ($n = 3$)	2	0	1	0
Adrenals ($n = 2$)	1	1	2	1
Lymph nodes ($n = 2$)	2	0	1	0
Bowel ($n = 1$)	0	0	0	0
Thyroid ($n = 1$)	1	0	0	0
Spinal cord ($n = 1$)	0	0	0	0
Total ($n = 31$)*	15	16	11	8

* On a per-patient basis, four patients had two organ metastases and three patients had metastases in three or more organs.

Bones and the lungs were frequent sites of false-positive interpretation at PET/CT, whereas bones and the liver were frequent sites of false-positive interpretation at whole-body MR imaging (Table 6). Bone lesions of osteophytes and fracture and lung lesions of benign inflammatory nodules simulated metastases at PET/CT. Bone lesions of vertebral hemangioma, flow-related enhancement, and marrow signal intensity changes associated with spondylosis and hepatic lesions of hemangioma and focal nodular hyperplasia mimicked metastases at whole-body MR imaging.

In retrospect, there were several metastatic lesions that reviewers failed to detect but were present on whole-body MR images—a bone lesion (mandible) in one patient, four lung metastatic nodules in three patients (small nodules < 10 mm in diameter), and two soft-tissue metastases in two patients.

Only PET/CT helped detect three

incidental papillary thyroid cancers and one glottic cancer. Both PET/CT and whole-body MR imaging allowed us to detect pituitary adenoma in one patient.

Discussion

Because it provides higher efficacy in T- and N-stage determinations than conventional staging methods (4), integrated PET/CT seems to be a first-line lung cancer staging tool. According to a report (15) in which the diagnostic efficacies of 1.5-T whole-body MR imaging and integrated PET/CT for the determination of staging accuracies for diverse malignant diseases were compared, T and N stages were more correctly diagnosed at integrated PET/CT than at whole-body MR imaging. However, in our study, there were no differences in efficacy of T- and N-stage determination between PET/CT and 3.0-T whole-body MR imaging. This finding was probably because of the use of a high-tesla (3.0-T) MR unit and phased-array cardiac coils for dedicated thoracic MR imaging. These conditions may have provided higher signal-to-noise ratio and thus higher contrast resolution in determining T and N staging with the 3.0-T MR imaging conditions (13,25). Kim et al (17) found sensitivity, specificity, and accuracy of 53% (39 of 74 nodal stations), 91% (453 of 496 nodal stations), and 86% (492 of 570 nodal stations), respectively, for hilar or mediastinal nodal metastasis detection at 3.0-T MR imaging in cases proved at surgery. These efficacy values are comparable to those for PET/CT for mediastinal nodal staging in NSCLC (18).

PET can help identify distant metastases that are not found by using traditional staging methods in 5%–20% of patients with NSCLC and can strongly influence treatment strategy and help predict survival (5–7). According to a report (26) in which whole-body MR imaging findings for the detection of bone metastases were directly compared with bone scintigraphy and FDG PET findings, whole-body MR imaging was found to have a higher sensitivity than skeletal scintigraphy for the detection of bone marrow metastases but a lower sensitivity than FDG PET. In contrast, in a study by Antoch et al (15), both modalities had comparable efficacy for metastasis detection. However, in a study by Schmidt et al (16), whole-body MR imaging was actually better for the detection of distant metastases. In our study, both modalities had similar performance for metastasis detection. However, the modalities had different advantages; whole-body MR imaging was better for detecting brain and liver metastases, whereas PET/CT was better for detecting lymph node and soft-

Figure 5

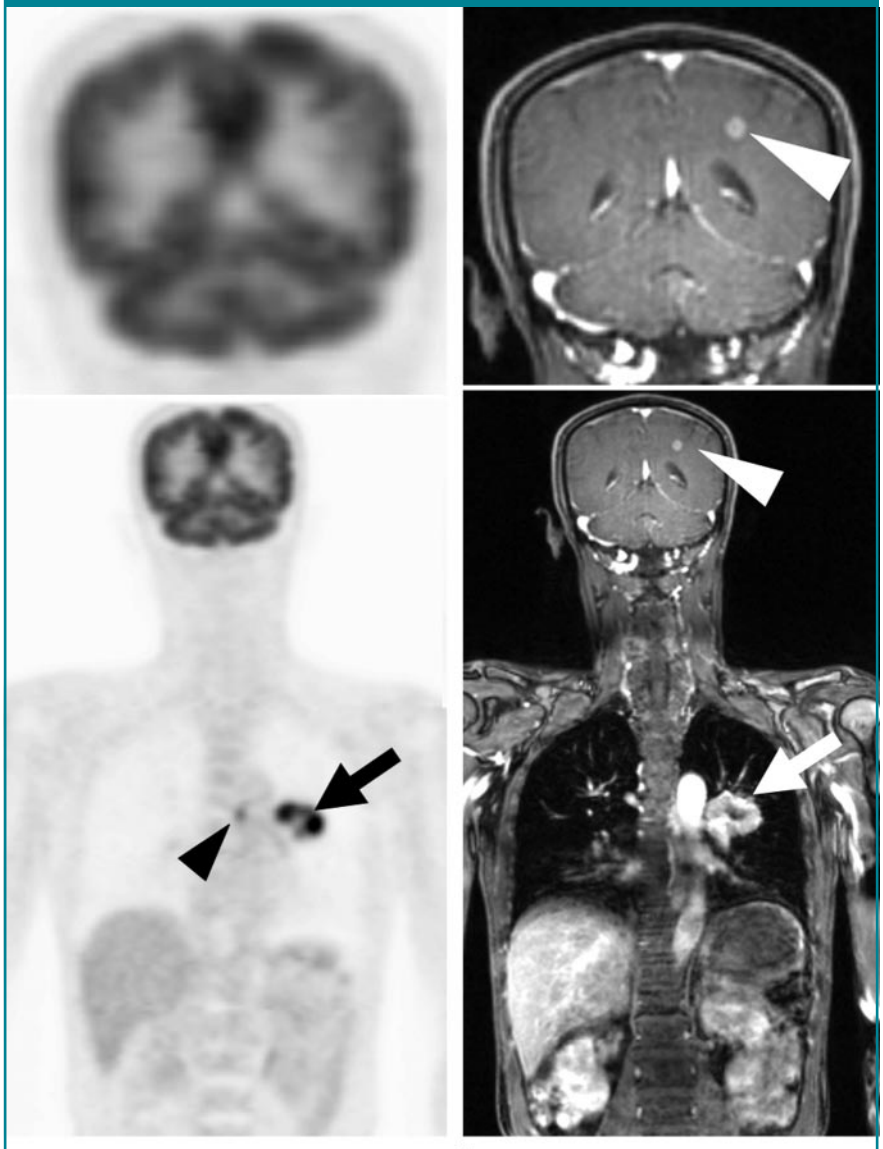

Figure 5: Images of brain metastasis in a 56-year-old man with NSCLC of the lung (with positive findings for aortopulmonary window [nodal station 5] and subcarinal nodal [nodal station 5] metastases, N2 disease) detected at whole-body MR imaging, but not at PET/CT. **(a)** Maximum intensity projection PET images show primary lung mass (arrow) in left upper lobe but not metastatic nodule in brain. Note FDG uptake in subcarinal node (arrowhead). **(b)** Enhanced T1-weighted turbo field-echo whole-body MR images show enhancing metastatic nodule (arrowheads) in left parietal lobe of brain. Note primary mass in left upper lobe (arrow). Increase in size on follow-up MR images confirms brain metastasis. Insets = targeted views of brain.

tissue metastases. The better contrast on MR images in specific areas, particularly in the brain, liver, and kidneys, may have allowed metastasis detection readily in these organs. Moreover, these organs show physiologic FDG uptake at PET that may have obscured metastatic lesion uptake.

In our study, both PET/CT and whole-body MR imaging had about 50% sensitivity for metastasis detection. It has been reported that PET does not depict microscopic metastases in about 20% of patients undergoing surgical therapy. Stroobants et al (7) identified that 16 (19%) of 86 patients undergoing a curative resection experienced a systemic relapse (unidentified microscopic metastasis with preoperative staging that included whole-body PET). In our study, metastases were confined to a single organ (or as a single small lesion) in a high percentage (68%) of patients, therefore reducing the sensitivity of both modalities. On the other hand, in our study, whole-body MR imaging resulted in several false-positive interpretations for bones and the liver, whereas PET/CT resulted in several false-positive interpretations for bones. False-positive interpretations resulted in further imaging studies or tissue characterization with biopsy.

With regard to subcentimeter lung nodule metastasis detection, the resolution of current PET scanners is only 5–6 mm in diameter (27). When one takes into account resolution and partial volume averaging effect, lung nodules up to 10 mm in diameter may not be characterized at PET or PET/CT. According to a recent report (14), 92% of small pulmonary noncalcified nodules of 5–10 mm in diameter were detected with a 3.0-T MR unit. If subcentimeter nodules carry cancer cells without calcification or fibrosis, these nodules can be more easily detected on T2-weighted TSE images because of exaggerated T2 contrast with a high-field-strength MR imaging condition. However, further studies need to be performed for subcentimeter nodule characterization by using either PET/CT or 3.0-T MR imaging.

For MR imaging, there are still remaining contraindications, such as metallic devices in the patient and claustrophobia. However, one major advantage of whole-body MR imaging is that it does not require radiation exposure, whereas the effective dose per integrated PET/CT examination can be as much as 25 mSv, a high exposure level for diagnostic imaging even with a low-dose CT technique (around 80 mA) for whole-body imaging (28).

Our study had several limitations. First, the majority of reference standard results, especially for M-stage determination, were not based on pathologic results but on results of clinical and imaging follow-up studies. Moreover, because we determined the presence of metastases by using results of follow-up imaging studies, from the statistical validity point of view, it might have been that the follow-up study had a false-positive result and the original study result was not a false-negative result and vice versa. Additionally, some of the metastases were detected as long as 10 months after the original study; thus, the lesions might be interval metastases and not false-negative cases. However, because original cancers were resected at surgery in most cases, we think the lesions were true rather than interval metastases. Second, no whole-body survey was conducted with these whole-body MR imaging or PET/CT during follow-up examinations, which may have weakened the reliability of negative results for either modality. Third, although we simplified the criteria for positive PET/CT interpretations, standard diagnostic criteria for a positive finding for metastasis in the extrathoracic organs are still in debate and are in an evolving stage. In addition, we did not obtain brain images by using a brain-specific technique. We do not exactly know if these limitations inflate or deflate the efficacy of these two modalities. It might be possible that the limitations may affect the absolute efficacy of PET/CT and MR imaging in the same direction so that their apparent difference is relatively unaffected. Fourth, for whole-body MR imaging, we had a relatively small field of view for an average-sized patient population and could not completely cover both upper arms. Furthermore, we obtained whole-body MR images in the coronal plane only. Therefore, lesions superficially located in the anterior or posterior body surfaces might not have been seen on MR images probably due to partial volume averaging.

In conclusion, both unenhanced PET/CT and 3.0-T whole-body MR imaging appear to provide acceptable accuracy and comparable efficacy for TNM staging of NSCLC, but for M-stage determination, each modality has its own advantages. Although the differences are not statistically significant, whole-body MR imaging is more useful for detecting brain and hepatic metastases, whereas PET/CT is more useful for lymph node and soft-tissue metastases.

Acknowledgment: The authors thank Seonwoo Kim, PhD, at Biostatistics Unit, Samsung Biomedical Research Institute, for her contribution to statistical analysis.

References

1. Pretreatment evaluation of non-small-cell lung cancer: The American Thoracic Society and The European Respiratory Society. Am J Respir Crit Care Med 1997;156:320–332.
2. Agress H Jr, Cooper BZ. Detection of clinically unexpected malignant and premalignant tumors with whole-body FDG PET: histopathologic comparison. Radiology 2004; 230:417–422.
3. Marom EM, McAdams HP, Erasmus JJ, et al. Staging non–small cell lung cancer with whole-body PET. Radiology 1999;212:803–809.
4. Dwamena BA, Sonnad SS, Angobaldo JO, Wahl RL. Metastases from non–small cell lung cancer: mediastinal staging in the 1990s—meta-analytic comparison of PET and CT. Radiology 1999;213:530–536.
5. Pieterman RM, van Putten JW, Meuzelaar JJ, et al. Preoperative staging of non-small-cell lung cancer with positron-emission tomography. N Engl J Med 2000;343:254–261.
6. MacManus MP, Hicks RJ, Ball DL, et al. F-18 fluorodeoxyglucose positron emission tomography staging in radical radiotherapy candidates with nonsmall cell lung carcinoma: powerful correlation with survival and high impact on treatment. Cancer 2001;92:886–895.
7. Stroobants SG, D'Hoore I, Dooms C, et al. Additional value of whole-body fluorodeoxyglucose positron emission tomography in the detection of distant metastases of non-small-

cell lung cancer. Clin Lung Cancer 2003;4:242–247.

8. Lardinois D, Weder W, Hany TF, et al. Staging of non-small-cell lung cancer with integrated positron-emission tomography and computed tomography. N Engl J Med 2003;348:2500–2507.
9. Shim SS, Lee KS, Kim BT, et al. Non–small cell lung cancer: prospective comparison of integrated FDG PET/CT and CT alone for preoperative staging. Radiology 2005;236:1011–1019.
10. Barkhausen J, Quick HH, Lauenstein T, et al. Whole-body MR imaging in 30 seconds with real-time true FISP and a continuously rolling table platform: feasibility study. Radiology 2001;220:252–256.
11. Lauenstein TC, Goehde SC, Herborn CU, et al. Whole-body MR imaging: evaluation of patients for metastases. Radiology 2004;233:139–148.
12. Schlemmer HP, Schafer J, Pfannenberg C, et al. Fast whole-body assessment of metastatic disease using a novel magnetic resonance imaging system: initial experiences. Invest Radiol 2005;40:64–71.
13. Tanenbaum LN. Clinical 3T MR imaging: mastering the challenges. Magn Reson Imaging Clin N Am 2006;14:1–15.
14. Yi CA, Jeon TY, Lee KS, et al. 3-T MRI: usefulness for evaluating primary lung cancer and small nodules in lobes not containing primary tumors. AJR Am J Roentgenol 2007;189:386–392.
15. Antoch G, Vogt FM, Freudenberg LS, et al. Whole-body dual-modality PET/CT and whole-body MRI for tumor staging in oncology. JAMA 2003;290:3199–3206.
16. Schmidt GP, Baur-Melnyk A, Herzog P, et al. High-resolution whole-body magnetic resonance image tumor staging with the use of parallel imaging versus dual-modality positron emission tomography-computed tomography: experience on a 32-channel system. Invest Radiol 2005;40:743–753.
17. Kim HY, Yi CA, Lee KS, et al. Nodal metastasis in non–small cell lung cancer: accuracy of 3.0-T MR imaging. Radiology 2008;246:596–604.
18. Kim YK, Lee KS, Kim BT, et al. Mediastinal nodal staging of nonsmall cell lung cancer using integrated 18F-FDG PET/CT in a tuberculosis-endemic country: diagnostic efficacy in 674 patients. Cancer 2007;109:1068–1077.
19. Shim SS, Lee KS, Kim BT, et al. Integrated PET/CT and the dry pleural dissemination of peripheral adenocarcinoma of the lung: diagnostic implications. J Comput Assist Tomogr 2006;30:70–76.
20. Mountain CF, Dresler CM. Regional lymph node classification for lung cancer staging. Chest 1997;111:1718–1723.
21. Kim YH, Lee KS, Primack SL, et al. Small pulmonary nodules on CT accompanying surgically resectable lung cancer: likelihood of malignancy. J Thorac Imaging 2002;17:40–46.
22. Gross BH, Glazer GM, Bookstein FL. Multiple pulmonary nodules detected by computed tomography: diagnostic implications. J Comput Assist Tomogr 1985;9:880–885.
23. O JH, Yoo IR, Kim SH, Sohn HS, Chung SK. Clinical significance of small pulmonary nodules with little or no 18F-FDG uptake on PET/CT images of patients with nonthoracic malignancies. J Nucl Med 2007;48:15–21.
24. Choi JY, Lee KS, Kwon OJ, et al. Improved detection of second primary cancer using integrated [18F] fluorodeoxyglucose positron emission tomography and computed tomography for initial tumor staging. J Clin Oncol 2005;23:7654–7659.
25. Lee VS, Hecht EM, Taouli B, Chen Q, Prince K, Oesingmann N. Body and cardiovascular MR imaging at 3.0 T. Radiology 2007;244:692–706.
26. Daldrup-Link HE, Franzius C, Link TM, et al. Whole-body MR imaging for detection of bone metastases in children and young adults: comparison with skeletal scintigraphy and FDG PET. AJR Am J Roentgenol 2001;177:229–236.
27. DeGrado TR, Turkington TG, Williams JJ, et al. Performance characteristics of a whole-body PET scanner. J Nucl Med 1994;35:1398–1406.
28. Brix G, Lechel U, Glatting G, et al. Radiation exposure of patients undergoing whole-body dual-modality 18F-FDG PET/CT examinations. J Nucl Med 2005;46:608–613.